Yusuke Katayama*, Shouichiro Iio*, Salisa Veerapun and Tomomi Uchiyama

Investigation of Blade Angle of an Open Cross-Flow Runner

Abstract: The aim of this study was to develop a nano-hydraulic turbine utilizing drop structure in irrigation channels or industrial waterways. This study was focused on an open-type cross-flow turbine without any attached equipment for cost reduction and easy maintenance. In this study, the authors used an artificial indoor waterfall as lab model. Test runner which is a simple structure of 20 circular arc-shaped blades sandwiched by two circular plates was used The optimum inlet blade angle and the relationship between the power performance and the flow rate approaching theoretically and experimentally were investigated. As a result, the optimum inlet blade angle due to the flow rate was changed. Additionally, allocation rate of power output in 1st stage and 2nd stage is changed by the blade inlet angle.

Keywords: cross-flow runner, blade angle, power performance, hydraulic turbine, MPS method

DOI 10.1515/tjj-2015-0005
Received February 16, 2015; accepted February 16, 2015

Introduction

In recent years, small-scale distributed hydropower systems utilizing unused water energy in irrigation and water-and-sewage infrastructures are being developed. There have been many researches about hydraulic turbines to utilize effectively small and distributed power systems, Darrieus turbine [1], gyro-type turbine [2] and others. These turbines are applicable for small stream, irrigation canals and water and sewage. It is thought that this approach could lead to cheaper power generation without environmental disruptions, compared with that produced by the large-scale and centralized hydroelectric plant. In this study we conducted basic experiments using a model turbine to realize waterfall-type turbines [3] that can be easily carried to, and installed on, the places where they are necessary, aiming at the utilization of small water energy. The flow through an impulse-type small-scale hydraulic turbine utilizing a waterfall of extra-low head is simulated by a two-dimensional Moving Particle Semi-implicit (MPS) method [4] and so on. The rotor performance is also analyzed by using the simulated flow field. In previous study, a positional relationship between the water flow and the runner was clarified [5], and the curved channel was investigated as flow direction control method [6].

In this paper, therefore, we conducted basic experiments such as measurement of power performance of the turbine and visualization of flow pattern, analyzed models and investigated the influence of the relationship between the blade inlet angle and power performance in order to understand the details of the power generation parameters in cross-flow turbines. In addition, numerical study was performed to clarify the detail of power-generating mechanism in waterfall-type turbine. It is important for improving the efficiency.

Experimental setup and procedure

Figure 1 shows an overview of the experimental setup. The experiment was conducted with an artificial waterfall made in a laboratory. The water in the lower tank is pumped up to the upper open channel and flows along the curved channel, then falls into the runners. In order to prevent the water perturbation issuing from the water supply pipe, we placed a sponge under the outlet of the pipe and rectified the water flow by narrowing the width of the water channel and making its depth shallower toward the falling point. The flow rate is controlled by a hand valve mounted downstream of the pump and is measured with an electromagnetic flow meter (Toshiba,

*Corresponding author: Yusuke Katayama, Department of Mathematics and System Development, Shinshu University, 4-17-1 Wakasato, Nagano 380-8553, Japan, E-mail: 13st201c@shinshu-u.ac.jp
Shouichiro Iio, Department of Environmental Science and Technology, Shinshu University, 4-17-1 Wakasato, Nagano 380-8553, Japan, E-mail: shouiio@shinshu-u.ac.jp
Salisa Veerapun, Department of Mechanical Engineering, Naresuan University, 99 Moo 9 Tambon Tha Pho, Muang, Phitsanulok 65000, Thailand, E-mail: salisav@nu.ac.th
Tomomi Uchiyama, EcoTopia Science Institute, Nagoya University, Furo-cho, Chikusa-ku, Nagoya 464-8601, Japan, E-mail: uchiyama@is.nagoya-u.ac.jp

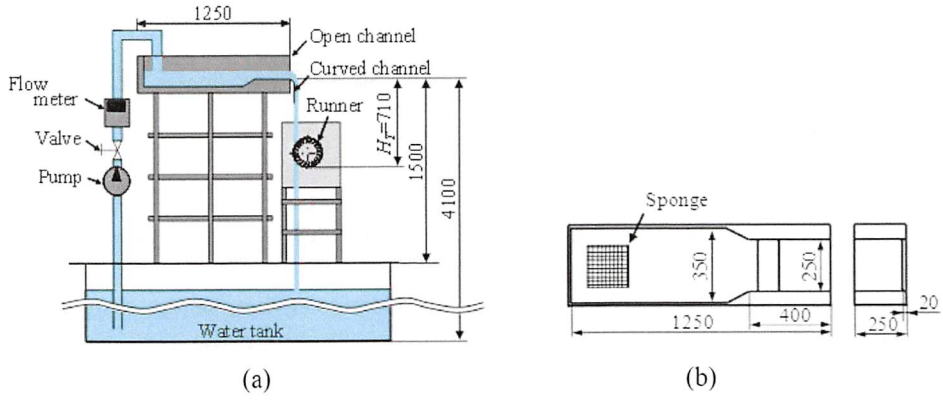

Figure 1: Experimental schematic. (a) Experimental setup. (b) Open channel.

LF400). The flow rate sets as $Q = 7.0 \times 10^{-3}$ m^3/s and included the error of ±0.5% in this study. The water level at the end of the open channel was $h_0 = 35$ mm, and its ratio with the runner diameter D_R (h_0/D_R) was 0.175. The water velocity was $V_0 = 0.8$ m/s. This open-type cross-flow turbine has no casings or nozzles, so the performance is significantly affected by the flow conditions. The relative position of the water flow and the runner is particularly important; thus, the position of the runner may be adjusted according to the drop position of the water flow. However, this method requires complicated auxiliary equipment. It is impractical because of the economic and maintenance considerations.

Figure 2 shows a detail of the curved channel. This curved channel allows control of the drop position of the water flow while maintaining fixed runner position. The configuration of the curved channel has a plate positioned tangentially and vertically downward to a quadrant starting at the open channel exit. The curvature radius was $R_c = 60$ mm, the distance between the curved channel and the runner shaft was $L_c = 85$ mm, and the length of the plate of the curved channel was $H_{pl} = 300$ mm. The origin of the coordinate system is in the center of the channel bottom at the open channel exit, with the x-axis in the horizontal direction, the y-axis along the width direction and the z-axis in the downward vertical direction. The total head length was $H_T = 710$ mm.

Figure 3 shows the cross-flow runner, which has a diameter $D_R = \varphi 200$ mm and a width $L_R = 100$ mm. Their basic shape was based on the Banki Turbine Design [7]. The inlet blade angle was altered in 3° increments within the range of $21 \leq \beta_1 \leq 30°$, while the outlet angle was fixed at $\beta_2 = 90°$ in this experiment. The thickness of the blade

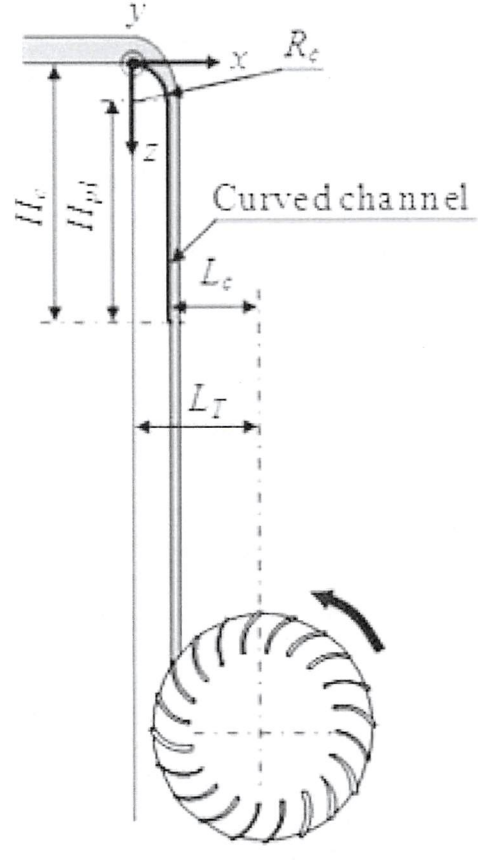

Figure 2: Flow direction control method.

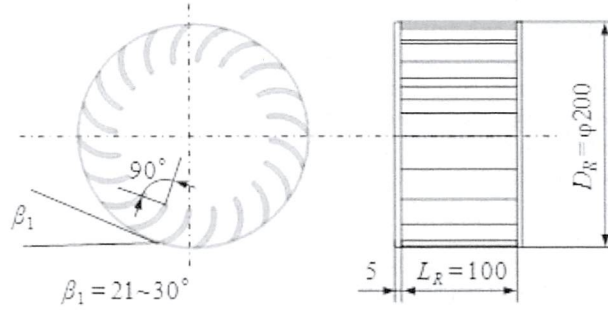

Figure 3: Runner configuration.

was $t_B = 3$ mm and the number of the blades was $n_B = 20$. The curvature of blade was changed with the inlet angle from 30.2 mm to 32.6 mm. A stainless steel shaft of $\varphi 15$ mm was installed through the center of the runner. The power output characteristics were evaluated by measurement of the rotation number and torque of the rotor axis. A powder brake (Mitsubishi Electric, ZKG-YN20) was used for loading, and the brake and torque meter (Ono Sokki, SS-050) were connected to the rotation axis via a coupling. The rotation number was measured with a magnetic detector (Ono Sokki, MP-981). The measurement started from the unloaded state and torque T and rotation number N were measured to calculate output P as the load was increased by the powder brake. The total error of the output power measurement is within 3%. The turbine efficiency η and tip speed ratio λ were defined with eqs (1–3).

$$\eta = P/\rho g Q(H_T + h_0) \quad [1]$$

$$\lambda = u_t/V_F \quad [2]$$

$$V_F = V_0 + \sqrt{2g(H_T - h_0/2)} \quad [3]$$

where P is the output, ρ is the density, g is the gravitational acceleration, u_t is the tip speed of the runner, V_F is the velocity of the water flow when it impinges the runner and h_0 is the water level at the origin.

Numerical analysis method and conditions

It is considered here that the flow through the hydraulic turbine is incompressible flow governed by the mass and momentum conservation equations:

$$\frac{D\rho}{Dt} = 0 \quad [4]$$

$$\frac{Du}{Dt} = -\frac{1}{\rho}\nabla p + \nu\nabla^2 u + F \quad [5]$$

where ρ, t, u, p and ν represent density, time, velocity, pressure and kinematic viscosity, respectively. F is the external force such as the gravitational force and the surface tension.

The authors have performed the numerical simulation for a waterfall-type nano-hydraulic turbine by the MPS method [4]. The fluid is discretized by particles, and the particle motion is computed by the Lagrangian method. Equations (4) and (5) are discretized through the interactions between the particles. This study simulates the flow through a cross-flow runner with the particle method.

The interactions between the particles are modeled with a weight function, w, defined by the following equation:

$$w(r) = \begin{cases} r_e/r - 1 & r \le r_e \\ 0 & r < r_e \end{cases} \quad [6]$$

where r is the distance between two particles, and r_e stands for a kernel size.

The particle number density at the position of the ith particle, n_i, is defined as

$$n_i = \sum_{j \neq i} w(|\boldsymbol{r}_j - \boldsymbol{r}_i|) \quad [7]$$

where r_i is the position vector of the ith particle.

As the fluid density remains unaltered in the incompressible flow, the particle number density is required to be constant. The incompressible flow condition in the MPS method is satisfied by maintaining n_i at a constant value n_0.

The Laplacian operator, expressing the viscous term on the right-hand side of eq. (5), is modeled with the weight function. The Laplacian operator at the position of the ith particle is given as

$$\nabla^2\phi_i = \frac{2d}{n^0\Lambda}\sum_{j \neq i}\left[\left(\phi_j - \phi_i\right)w(|\boldsymbol{r}_j - \boldsymbol{r}_i|)\right] \quad [8]$$

where ϕ is a physical quantity. A parameter Λ is introduced such that the variance increase is equal to the analytical solution:

$$\Lambda = \int_V w(r)r^2 dv \Big/ \int_V w(r) dv \quad [9]$$

The gradient operator, expressing the pressure gradient term on the right-hand side of eq. (5), is also modeled. The gradient operator at the position of the ith particle is modeled by setting the interparticle force at the repulsion to ensure the numerical stability [8, 9]. Thus, the interacting pressure forces between two particles are not antisymmetric, and the momentum is not always conserved. To resolve this problem, this simulation employs the following model presented by Khayyer and Gotoh [10].

$$\nabla\phi_i = \frac{d}{n^0}\sum_{j \neq i}\left[\frac{\left(\phi_i + \phi_j\right) - \left(\hat{\phi}_i + \hat{\phi}_j\right)}{|\boldsymbol{r}_j - \boldsymbol{r}_i|^2}(\boldsymbol{r}_j - \boldsymbol{r}_i)w(|\boldsymbol{r}_j - \boldsymbol{r}_i|)\right] \quad [10]$$

where d is the number of space dimensions, and $\hat{\phi}_i$ is defined as

$$\hat{\phi}_i = \min_{j \in J}\left(\phi_i, \phi_j\right), \quad J = \{j : w(|\boldsymbol{r}_j - \boldsymbol{r}_i|) \neq 0\} \qquad [11]$$

Equations (4) and (5) are solved by a semi-implicit method, which is used in the SMAC method [11]. When the particle velocity $\boldsymbol{u}_i^k$ and position $\boldsymbol{r}_i^k$ at time $t = k\Delta t$ are known, the flow at time $t = (k+1)\Delta t$ is simulated by the following two steps.

First, the temporal velocity and position for the particle $\boldsymbol{u}_i^*$ and $\boldsymbol{r}_i^*$ are calculated from eq. (5) without considering the pressure gradient term. Then, the temporal particle number density n_i^* is computed using eq. (7).

Second, the following Poisson equation is solved for the pressure p^{k+1} provided that the mass conservation is satisfied or n_i^* coincides with n^0.

$$\nabla^2 p_i^{k+1} = -\frac{\rho}{\Delta t^2}\frac{n_i^* - n^0}{n^0} \qquad [12]$$

Then, the temporal velocity and the position of the particle are corrected by the obtained pressure gradient.

$$\boldsymbol{u}_i^{k+1} = \boldsymbol{u}_i^* + \boldsymbol{u}_i' \qquad [13]$$

$$\boldsymbol{r}_i^{k+1} = \boldsymbol{r}_i^* + \boldsymbol{u}_i'\Delta t \qquad [14]$$

$$\boldsymbol{u}_i' = -\frac{\Delta t}{\rho}\nabla p^{k+1}{}_i \qquad [15]$$

The viscous term in eq. (5) and the left-hand side of eq. (12) are computed by the Laplacian operator, eq. (8). The right-hand side of eq. (15) is calculated by the gradient operator, eq. (10).

This study simulates the flow by the two-dimensional MPS method. The computational domain is illustrated in Figure 4: 3.5 D_R in the x direction and 1.51 D_R in the z direction. The water thickness t and velocity V_0 upstream of the runner are 10 mm and 3.0 m/s, respectively. In this calculation, the flow is issued from inlet region as a water jet which has flat velocity distribution.

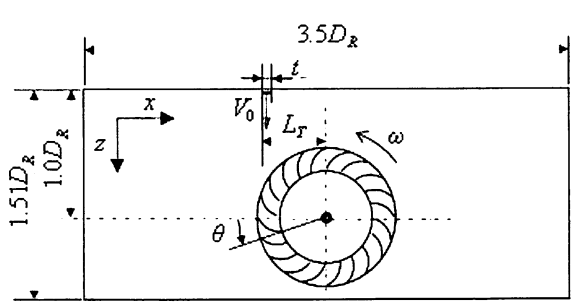

Figure 4: Computational domain.

The water jet velocity is set based on the experimental value. The clearance L_T is 87 mm at which the highest efficiency is obtained. The simulation is conducted at the conditions of $0.1 \leq \lambda \leq 0.8$.

The particles, discretizing the waterfall, are released from the upstream boundary into the computational domain with the velocity V_0. It is required that the released particles are uniformly arranged at interval l_0 in the horizontal and vertical directions to ensure the computational accuracy. The blade and the runner shaft, which are the solid walls, are also discretized by the particles. The distance between these particles is also set at $l_0/t = 0.099$, from the previous numerical simulation result by Uchiyama et al. [4]. The static pressure is given on the downstream boundary ($x/D_1 = 2$). The traction-free condition is assumed on the other boundaries.

The pressure is set at zero on the free surface. The position of the free surface is detected according to the particle number density. When the particle number density n_i^* calculated at the first step of each time step satisfies the following relation, the ith particle is decided presenting on the free surface.

$$n_i^* < \beta n^0 \qquad [16]$$

where β is a parameter of $\beta < 1$. The time increment Δt is 5×10^{-5} s. The value of r_e in eq. (6) is generally chosen at $2 \leq r_e/l_0 \leq 4$ [8, 9]. The value for the particle number density and the gradient operator is $2.1l_0$, while it is $4l_0$ for the Laplacian operator [8]. The parameter β in eq. (16) is set at 0.97. It is reported that the simulation of a fragmentation of fluid scarcely depends on the β value in the case of $0.8 \leq \beta \leq 0.99$ [9]. The power performance was evaluated based on angular momentum theory. The details of the power-generating mechanism of the first and second stages (hereafter referred to as 1st stage and 2nd stage, respectively) were determined, which had been difficult to measure experimentally. The efficiency of both stages was also calculated.

Experimental results and discussion

Experimental results

Figure 5 shows the power performance for various β_1 angles. The distribution shape of the power performance scarcely changed with difference β_1. However, the unloaded rotating speed increased, and the η also

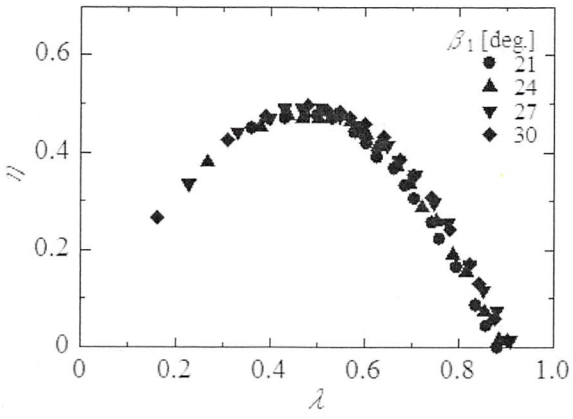

Figure 5: Power performance (experiment).

increased as the β_1 increased in detail. In the experiment, the maximum efficiency $\eta = 0.498$ was obtained when $\beta_1 = 30°$.

Calculation results

The experimental results show that the turbine efficiency η changes depending on the tip speed ratio λ, obtaining maximum efficiency (η_{max}) when $\lambda = 0.5$. Figure 6 shows visualization of flow pattern at $\beta_1 = 30°$, and $\lambda = 0.5$. The water flow fell into the runner and impinged the blades. The water passed through inside the runner and hit the blades again. Figure 7 shows the instantaneous distribution of the particles by MPS method corresponding with Figure 6.

Figure 8 shows time-averaged velocity distribution. Most of the water flow hits the blade at the concave side and flows into the runners (position A in the figure). Then the water flow passes through the inside of the runner and hits the other blades again below the runner shaft (position B in the figure). The water flow velocity

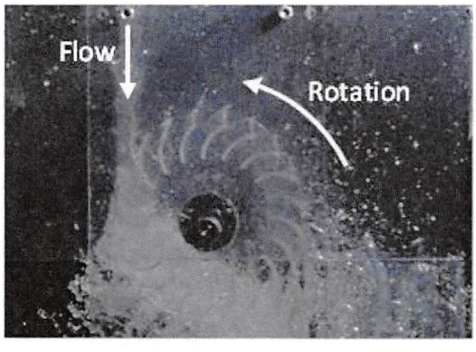

Figure 6: Visualization of flow pattern (Exp. $\beta_1 = 30°$, $\beta_2 = 90°$, $\lambda = 0.5$).

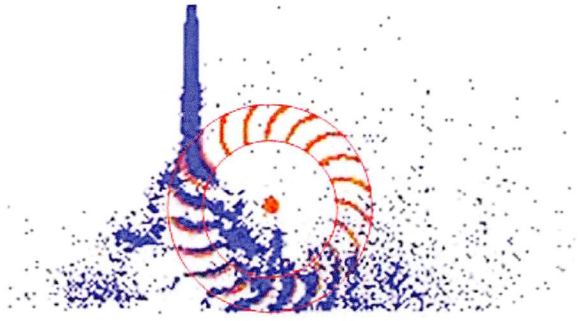

Figure 7: Particle distribution (Cal. $\beta_1 = 30°$, $\beta_2 = 90°$, $\lambda = 0.5$).

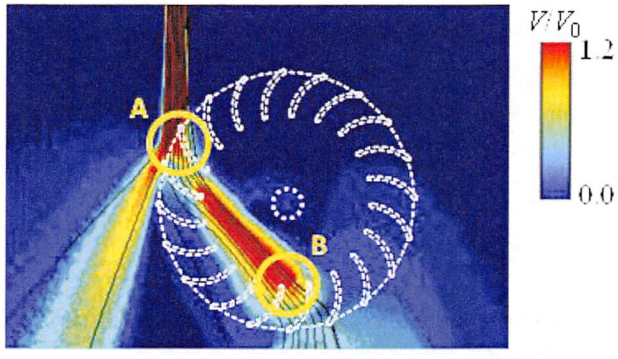

Figure 8: Velocity distribution and streamline ($\beta_1 = 30°$, $\beta_2 = 90°$, $\lambda = 0.5$).

decreases after passing the blades which indicates that the torque is applied to the runner. Some of the water flow hits the convex side of the blade at position A and deflects to the outside of the runner. As shown in Figure 8, the water acts on the runner twice, which is a distinctive feature of cross-flow turbine. The region of water flow through the blade outside to inside (position A in the figure) is called the 1st stage, and the region of water flow through the blade inside to outside (position B in the figure) is called the 2nd stage. The intersections of streamline that passes through the center of the water flow with the outer and inner circumferences of the runner were labeled as points 1 to 4 in Figure 9. Figure 9 shows the velocity triangles of this cross-flow turbine. The output, P_{1st} and P_{2nd} at each stage, was calculated using the angular momentum theory based on the absolute velocity and the runner tip speed at each point. The outputs at each stage and the total output were defined as eqs (17–19) as follows:

$$P_{1st} = \rho Q(V_{1\theta}\, u_{t1} - V_{2\theta}\, u_{t2}) \quad [17]$$

$$P_{2nd} = \rho Q(V_{3\theta}\, u_{t3} - V_{4\theta}\, u_{t4}) \quad [18]$$

$$P_{all} = P_1 + P_2 \quad [19]$$

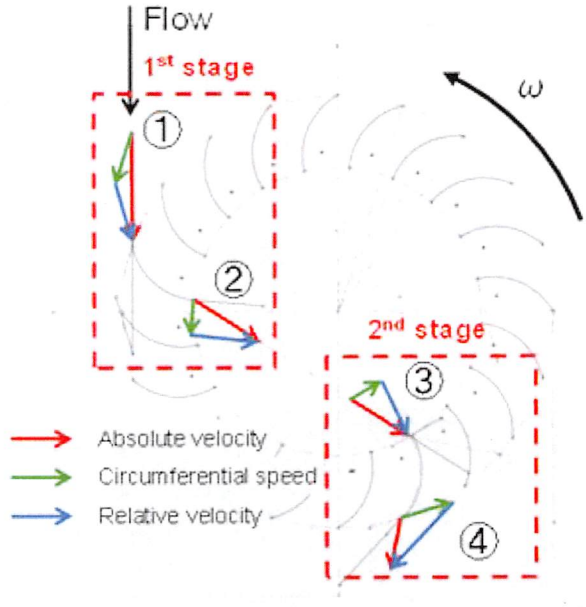

Figure 9: Velocity triangles.

Here subscript θ denotes the component in the circumferential direction.

The power performances of the difference blade inlet angle β_1 are shown in Figure 10. The open marks represent the efficiency at each stage, and the solid marks represent the total efficiency. When the inlet angle is $\beta_1 < 27°$, the output in the 2nd stage is greater than that in the 1st stage. When $\beta_1 = 27°$, both stages produce almost same outputs, and when $\beta_1 > 27°$, the 1st stage prevails in output. The torque acting on the blades by water flow was enhanced as β_1 increased because the blades become perpendicular to the water flow with increasing β_1 in the 1st stage. When water flow discharges toward outside of runner blades, circumferential component of the water flow velocity becomes smaller as β_1 is smaller for the 2nd stage. The relationship between the efficiencies on total and each stage and β_1 is shown in Figure 11. The η of each stage is defined by the ratio of the output of each stage relative to the energy of the entire water. The η of 1st stage is rising with increasing the β_1. On the other hand, η of 2nd stage has peak point at $\beta_1 = 27°$. The mechanism of power generation was revealed. Figure 12 shows the comparison between experimental and numerical results. The calculated value of η is smaller than the experimental value. This may be explained by comparing Figures 6 and 7, which show that while most of the water flows inside the runners (Figure 6), some of the water flow hits the convex surface of the blade and is deflected to the outside of the runner

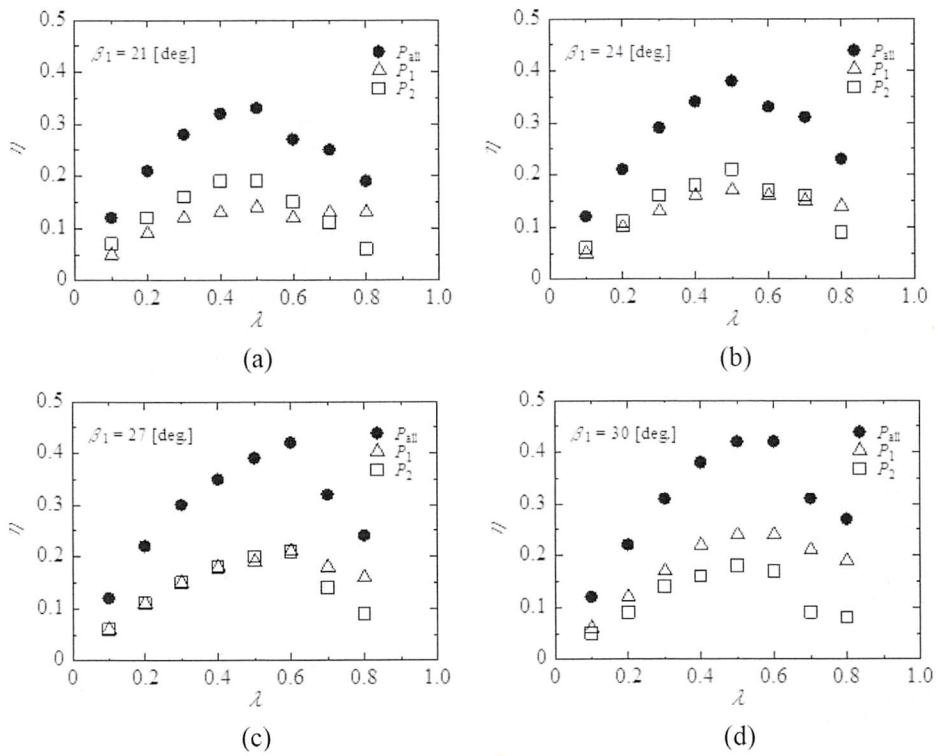

Figure 10: Power performance (MPS method). (a) $\beta_1 = 21°$; (b) $\beta_1 = 24°$; (c) $\beta_1 = 27°$; (d) $\beta_1 = 30°$.

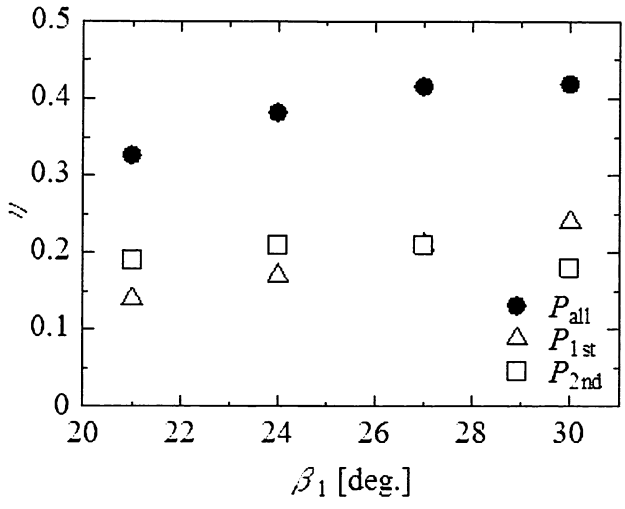

Figure 11: Efficiency of each stage.

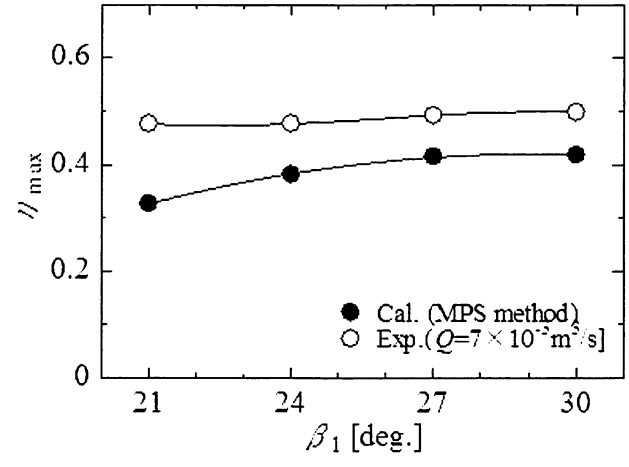

Figure 12: Comparison of experiment and calculation for η_{max}.

in the particle distribution (Figure 7). There is a tendency in which the smaller the β_1 value, the greater the proportion of the convex side relative to the direction of the water flow, increasing the volume of the flow that is deflected to the outside of the runner. Accordingly, differences between the experimental results and calculations increase as the value of β_1 decreases because the amount of water flowing into the runners decreases. In both cases, the approximation curve shows local maximum values at $\beta_1 = 29°$.

Conclusions

This paper examined an open-type cross-flow turbine to determine how the blade inlet angle affects power performance. The obtained results are as follows:

1. The distribution rate of the output between the 1st and 2nd stages depends on the inlet angle of the runner blade.
2. While the output ratio of the 1st stage is high when the β_1 value is small, that of the 2nd stage is high when the β_1 value is large.
3. With a flow rate of $Q = 7.0 \times 10^{-3}$ m^3/s, the optimum inlet angle of the runner blade is $\beta_1 = 29°$ in both the experimental and calculated cases.

Nomenclature

D_R	Runner diameter, mm
h_0	Water level at end of open channel, mm
L_C	Distance between curved channel and runner shaft, mm
L_R	Width of runner, mm
N	Rotation number, rpm
P	Power output from, W
Q	Flow rate, m^3/s
T	Torque of runner, Nm
u_t	Tip speed, m/s
V_0	Water velocity at end of open channel, m/s
V_F	Impinging velocity, m/s
β_1	Inlet blade angle, degree
β_2	Outlet blade angle, degree
η	Turbine efficiency
λ	Tip speed ratio

Funding: This work was supported by JSPS Fellows Grant Number 2510285, JSPS KAKENHI 26820043 and the joint research program of the EcoTopia Science Institute, Nagoya University.

References

[1] Shimokawa K, Furukawa A, Okuma K, Matsushita D, Watanabe S. Side-wall effect of runner casing on performance of Darrieus-type hydro turbine with inlet nozzle for extra-low head utilization. Sci China Technol Sci 2010;53(1):93–9.

[2] Kanemoto T, Inagaki A, Misumi H, Kinoshita H. Development of gyro-type hydraulic turbine suitable for shallow stream (1st report). Trans JSME Ser B 2011;70(690):413–18.

[3] Ikeda T, Iio S, Tatsuno K. Performance of nano-hydraulic turbine utilizing waterfalls. Renew Energ 2010;35(1):293–300.

[4] Uchiyama T, Fukuhara H, Iio S, Ikeda T. Numerical simulation of water flow through a nano-hydraulic turbine of waterfall-type by particle method. Int J Rotating Mach 2013;2013:Article ID 473842:1–8.

[5] Oike S, Yamazaki M, Iio S, Ikeda T. Investigation of open type cross-flow runner performance utilized for waterfall type hydraulic turbine. Turbomachinery 2011;39(3):177–83. in Japanese

[6] Iio S, Oike S, Yamazaki M, Kimoto M, Katayama Y, Ikeda T. Study on a waterfall type hydraulic turbine: investigation of a flow direction control method by using a curved channel. Turbomachinery 2012;40(12):745–53. in Japanese

[7] Mockmore CA, Merryfield F. "The Banki Water Turbine", Bulletin Series, 25, Engineering Experimental Station, Oregon State System of Higher Education, Oregon State College, Corvalis, 1949.

[8] Koshizuka S, Nobe A, Oka Y. Numerical analysis of breaking waves using the moving particle semi-implicit method. Int J Numer Meth Fluids 1998;26:751–69.

[9] Koshizuka S, Oka Y. Moving-particle semi-implicit method for fragmentation of incompressible fluid. Nucl Sci Eng 1996;123:421–34.

[10] Khayyer A, Gotoh H. Development of CMPS method for accurate water-surface tracking in breaking waves. Coast Eng J 2008;50 (2):179–207.

[11] Amsden AA, Harlow FH. A simplified MAC technique for incompressible fluid flow calculations. J Comput Phys 1970;6(2):322–5.